water

MDPI

Article

Investigating the Influence of Vegetation Height on the Air Concentration of Supercritical Aerated Flows

Anne Mozer * and **S. Harish**

Institute of Hydraulic Engineering and Water Resources Management, RWTH Aachen University, Mies-van-der-Rohe-Straße 17, 52056 Aachen, Germany; selvam@iww.rwth-aachen.de
* Correspondence: mozer@iww.rwth-aachen.de

Abstract: Spillways can present a way to control the overflowing of water during flood events and prevent damage from levee breaches. With increasing interest in nature-based solutions, the interaction between flow and vegetation parameters has to be understood. Aeration usually occurs during the overflow of sloped spillways, leading to the bulking of flow, alterations of flow characteristics, and energy dissipation. The influence of the vegetation parameter on aerated flow characteristics has not yet been investigated in greater detail; no systematic investigation of the effect of vegetation parameters has been conducted. This paper aims to systematically analyze the influence of different vegetation heights on air entrainment during the overflow of spillways. Therefore, a spillway model with a slope of 18° (1:3) was equipped with artificial turf of varying turf heights, and supercritical flows were investigated. The aeration was measured using double-tip conductivity probes, giving insights into air concentration profiles, bubble count rates, estimations of energy dissipation, and flow velocities. The results highlighted the significant influence of vegetation height on the aeration process. Higher air concentrations over the flow depth were observed for higher turf heights tested in this study. Also, the energy dissipation and flow velocity reduction increased with higher vegetation heights. Overall, the present study uncovers the effect of vegetated covers, thereby contributing to the fundamentals of aerated flows.

Keywords: air–water flow; aeration; high-velocity flow; nature-based solution; vegetation; two-phase flow

Citation: Mozer, A.; Harish, S. Investigating the Influence of Vegetation Height on the Air Concentration of Supercritical Aerated Flows. *Water* **2024**, *16*, 3136. https://doi.org/10.3390/w16213136

Academic Editor: Bommanna Krishnappan

Received: 17 September 2024
Revised: 25 October 2024
Accepted: 30 October 2024
Published: 1 November 2024

1. Introduction

The predicted changes in climate imply a challenge for water management in terms of flood protection. These changes can cause increased precipitation intensity, river flooding, and water temperature changes that can affect the ecosystem. In the case of riverine floods, the high water levels in rivers can cause the overflowing of water, which can cause levees to breach, potentially leading to massive flooding and damage. The potential damage to the hinterland in the case of a levee breach increases the damage caused by the controlled spillway overflowing [1]. In addition, if the overflowing water energy is not dissipated, the overflowing flow's kinetic energy can significantly damage the levees [2]. Thus, it is advisable to provide levees with spillways to control the flow rate and overtopping during floods [3].

Spillways can be smooth, rough, or stepped chutes, usually made of concrete structures. The most common solution is concrete riprap [3]. Nature-based solutions aim for ecological and environmentally friendly solutions, such as providing levees with a grassed top layer instead of concrete. They provide environmental benefits such as biodiversity conservation and can improve resilience to flood risks. Further, they are conventionally used on hydraulic structures like embankments, river banks, floodplains and dams, in addition to spillways and levees, to stabilize the soil and reduce erosion [4–6]. A better understanding of nature-based solutions can help maximize the advantages and provide a more sustainable and effective management strategy by increasing the ecological value for both nature and humans [7,8]. For example, nature-based solutions can act as carbon sequestration and thereby reduce carbon emissions [9]. Furthermore, nature-based solutions help maintain the natural hydrological cycle of evapotranspiration and are able to intersect water in case of rainfall, mitigating floods by reducing runoff [10,11]. With increasing interest in nature-based solutions and, thus, dikes being constructed with a vegetated top layer, the interaction between vegetation cover and water overflow must be understood.

1.1. Overflowing Process and the Onset of Aeration

When water overflows the chute of a spillway, the water is clear and usually non-aerated at the upstream end. The water is accelerated due to gravitation, which increases the flow velocity [12]. A boundary layer is developed along the chute, consisting of a sloped path. Flow fluctuations increase in the following section [13]. As soon as the outer edge of the boundary layer reaches the free surface and the effects of surface tension and buoyancy are overcome, air starts to entrain into the water flow, and the flow becomes fully aerated [14–18]. The inception point is where the self-aeration starts [15,18], a critical spillway design parameter for predicting energy dissipation, flow depth, and air entrainment [19]. At this point, turbulence shear stresses next to the free surface exceed surface tension and buoyancy forces [20,21]. The inception point is usually found at a characteristic level of tangential Reynolds stresses next to the free surface. At the point of air entrainment, undulations and underlying eddies can be observed [22]. Air bubbles are entrained into the flow due to intense turbulent shear at the free surface at the inception point, at which the turbulent shear stress exceeds the capillary force, resulting in a free surface breakup and bubble entrapment [22]. The inception point can be identified through the appearance of "white water" [23,24].

Directly downstream of the inception point, large amounts of air are entrained, which results in a highly varied flow [21]. The amount of air in the fluid gradually increases along the chute [20]. An equilibrium status is reached downstream of the inception point, in which the aeration respective to the amount of air does not change [14,25]. The properties are no longer dependent on the distance along the spillway [23,26]. The mean void fraction, flow depth, and mean velocity are constant along the spillway when the equilibrium condition is reached [25]. Figure 1 shows a schematic drawing of the air entrainment process during the spillway overflow.

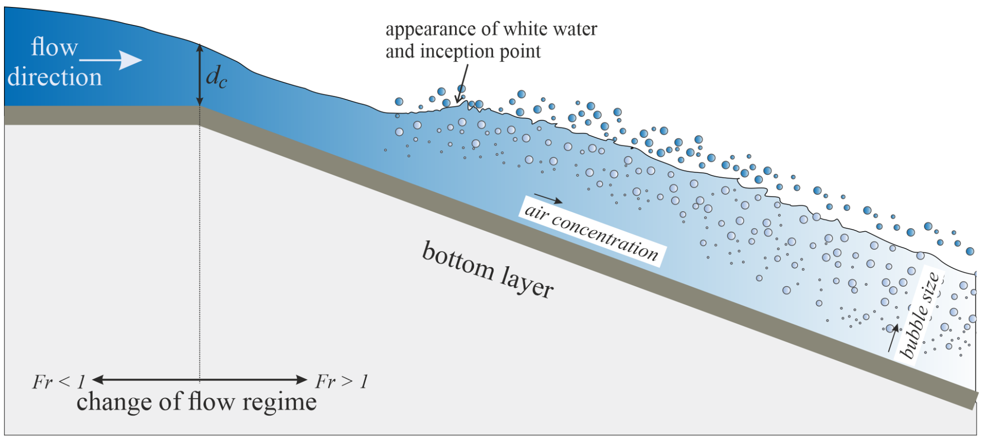

Figure 1. A schematic drawing of the process of air entrainment over a spillway chute (not to scale) (based on [17]).

Aeration leads to the bulking of the flow [18], the alteration of flow dynamics, and energy dissipation [14]. However, aeration can also help to protect the boundary from cavitation damage [20]. The different stages of the self-aeration process differ in mean air concentration [13]. Within a cross-section, the size of the air bubbles varies from small close to the bottom to large near the free-surface area [17]. In particular, three layers can be observed. The top layer contains air and a few water droplets; the middle layer can be described as a mixture of air and water; and the bottom layer consists of water and a few air bubbles [27]. The void fraction, therefore, amounts to between 0 and 100%, where a void fraction of 0 % can be found at the bottom layer, and 100 % refers to the atmosphere [23].

Straub and Anderson (1958) [28] were among the first to investigate the effect of aeration on spillways. Several studies on stepped and smooth spillways were conducted [2,21,23,29–31]. However, vegetated spillways have not yet been investigated thoroughly, with only a few studies giving insights into vegetation and aeration [13,14,16,32].

1.2. Vegetation and Flow Parameter

Vegetation provides ecological value and ecosystem services, such as promoting the retention of particles and sedimentation due to the creation of areas with reduced bed stress and increasing habitat diversity as well as water quality [33–35]. At the same time, vegetation influences the flow velocity and alters the flow characteristics, presenting a common flow barrier [34–37]. Vegetation can lead to a hydraulic jump as the supercritical flow enters the vegetation canopy and is forced to slow down. In general, hydraulic jumps usually appear if, e.g., the bed elevation suddenly changes, which can be due to vegetation [38,39]. The presence of vegetation increases flow and friction resistance to overflowing water [33,38] while reducing velocity and boundary shear stress [14]. Due to the induced reduction in the flow velocity, a velocity gradient between the vegetated and non-vegetated area in the flow section is generated, influencing the flow's stability and turbulence characteristics and promoting turbulence dissipation [40].

The influence of vegetation on flow properties depends on several parameters, including vegetation height, the grade of vegetation cover, and roughness. Furthermore, water depth and flow velocity have been found to impact friction and flow resistance [33,40]. The submergence ratio sets flow depth and vegetation height in relation with each other. It was found that the submergence ratio correlates negatively with friction and resistance. Thus, increasing the flow depth relative to the vegetation height reduces the overflowed vegetation's friction factor and flow resistance [32,37]. However, flow depths exceeding the vegetation height and higher flow velocities cause tilt and bending of the vegetation. Especially for high slopes on overflowed embankments, high flow velocities result in tilted vegetation, resulting in a comparatively smooth surface [41]. Thus, the vegetation height also influences the roughness of the vegetated surface.

Another parameter influencing the flow characteristics is the grade of coverage of the vegetation surface. The flow resistance is expected to decrease with reduced vegetation cover, which is caused by increased flow velocity and the decreased momentum exchange in the sections between the individual plants. With lower vegetation coverage, the area between the individual plants increases, which results in a more significant flow velocity [32], and thus, the velocity gradient between vegetated and non-vegetated areas in the flow section increases [40,42]. A lower flow resistance was found for increasing flow velocity. Furthermore, for high flow velocities, the vegetation density was found to play a minor role, and differences in flow resistance were decreased between variations of vegetation densities [43]. Different studies have been conducted so far on different topics of interaction between vegetation and flow. This includes the investigation of dikes, rivers, or channels e.g., [16,34,43,44].

1.3. Vegetation and Aeration

Similar observations regarding the aeration process on overtopping chutes described previously were made in studies on vegetated spillways. The upper part of the chutes was mostly unaerated, with an aeration starting point observed at a particular location, where the air started to get mixed into the flows, and surface tension was overcome due to turbulences [16]. Vegetation on chutes promotes the aeration processes of the flow and the mixing of air into water [14]. With an increasing roughness height, the turbulent boundary layer grows faster; thus, the inception point moves closer to the crest [14]. It was found that aeration characteristics (e.g., bubble size) change with different types and changing flexibilities of vegetation [14]. However, the air concentration showed a typical distribution along the chute, with lower air concentration directly downstream of the inception point and higher air concentration at the chute's downstream end. Quasi-uniform conditions were observed towards the downstream end of the chute [32].

Experiments on vegetated spillways have shown that the presence of vegetation on the spillway increases the amount of energy dissipation [13,14] and promotes aeration of the flow [14,45]. The position of the inception point is altered with the changing roughness height [14]. Furthermore, past studies have clearly indicated that the contributing vegetation parameters significantly influence flow characteristics. Of these, the least concentrated are the effects of different vegetation heights, which could substantially influence aerated flow characteristics over vegetation.

Thus, this paper aims to increase the understanding of the process and effects of aeration on vegetated spillways in terms of vegetation height. Therefore, experiments were conducted on vegetated spillways of varying vegetation heights. Specifically, this study provides novel insights into the effect of different vegetation heights on the inception point location, the air concentration along the length of the chute, the energy dissipation for different vegetation heights, and flow velocity alteration by comparing it with a non-vegetated smooth chute.

2. Materials and Methods

2.1. Facility and Instrumentation

The experiments in this study's context were conducted in the Institute of Hydraulic Engineering and Water Resources Management (IWW) laboratory at RWTH Aachen University in a 0.5 m wide spillway facility (see Figure 2). The spillway's crest was 1.8 m high, and the embankment had an angle of 18° (1:3 slope), which was based on the commonly adapted slopes on levees and dikes in Germany (DIN 19712 [46]). It was constructed from PVC used in the smooth-bottom experiments. The artificial turf layers were placed on top of the PVC for the remaining experiments. The model was constructed at a 1:1 scale, representing a medium-height dike system while disregarding erosion or root systems.

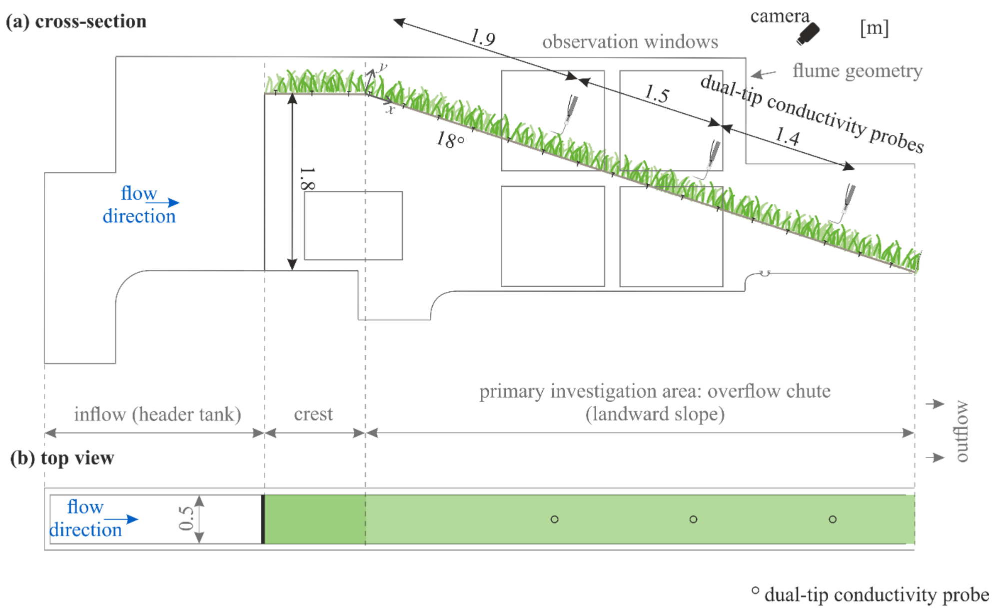

Figure 2. The setup of the model tests and measuring instruments: (**a**) cross-section and (**b**) top view.

The water flow was supplied from a header tank that pumps water into an upstream reservoir, which provided steady inflows into the test section. The flow rate was controlled via valves at the inflow into the upstream reservoir. The facility's water cycle is closed-circuit. The water enters the underground storage and is pumped back into the header tank and the spillway facility.

In the experiments, the influence of vegetation on the entrainment of air into supercritical flows down embankments was determined. Due to air entrainment, many measuring instruments become impractical and yield inaccurate measurements [47]. Thus, the presence of air in the flow requires special measurement techniques, such as using conductivity probes [31,48,49].

The measuring principle of conductivity probes is based on the difference in the electrical resistivity between water and air [47]. If the needle is in contact with air, the voltage drops due to air's greater resistivity than water [47,50]. This way, the signal can be processed, and the air phases can be obtained in the flow. Furthermore, the interfacial flow velocity can be calculated by determining the air bubbles at two needle tips separated by a fixed streamwise and transverse direction [14,47,51]. While double-tip conductivity probes are a common method for measuring air concentration, flow velocity, and bubble count, the inaccuracy level remains uncertain. Studies have found a reliable measurement of air–water flow properties in high-velocity flows above 3 m/s. Bubbles were found to slow down or deform in experiments with flow velocities lower than 2 m/s [52]. In the present study, the mean velocity varied between 1.9 m/s and 5.1 m/s, and hence, the measurements could be recognized as reliable with the conductivity probe. Furthermore, only one conductivity probe was used, and it was shifted along the slope in this study. Thus, the intrusive effects of the probe did not affect downstream measurements. Still, irregular bubble shapes or small bubbles pose a challenge when detecting phase changes.

Air–water flow measurements were determined using double-tip conductivity probes at three measuring positions covering the entire length of the chute. The measuring positions were at x = 1.9 m, 3.4 m, and 4.8 m from the crest. The probes were constructed at the institute. Each probe tip consisted of an inner electrode (diameter d = 0.13 mm) of platinum–iridium with Teflon insulation and an outer electrode of stainless steel. Epoxy resin served as an insulating and sealing material. Two of these tips were mounted in a 3 mm diameter VA steel tube. An acrylic glass case served as a holder for this VA steel tube (see Figure 3a) [31]. The double-tip conductivity probe comprised two needle tips separated by $\Delta x \approx 5$ mm in the longitudinal direction and $\Delta z \approx 1$ mm in the transverse direction (see Figure 3b).

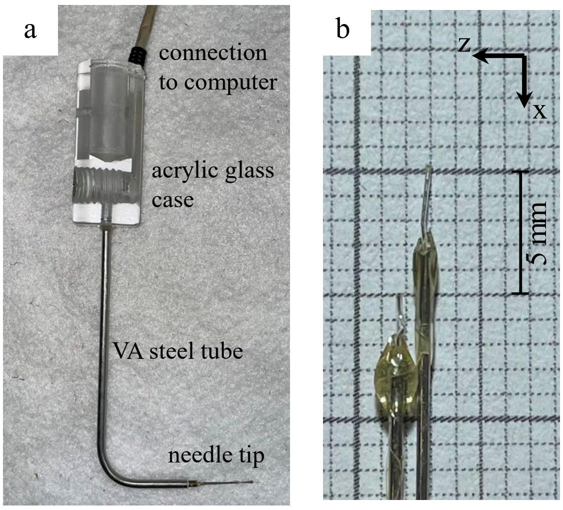

Figure 3. (**a**) A double-tip conductivity probe and its compartments, (**b**) the detail of the two needle tips.

The sensors were sampled at 40 kHz for 90 s at each measuring position. The conductivity probes were shifted upwards in the y-direction by every mm using a rack and pinion with a pitch error of 0.1 mm to sense the development of air entrainment over the flow depth. From the voltage signal, the air concentration and bubble count frequency could be derived by converting the voltage signal into a binary void fraction using a single threshold. With that, the air concentration over the sampling time could be calculated from the length of the entire signal and the length of the signal previously assigned to the air phase [50,53,54].

The adaptive-window cross-correlation (AWCC) method by Kramer et al. (2018) [54] was used to process the raw data. This method divides the signal from the double-tip conductivity probe into short time windows, each containing data for only a few bubbles.

It then applies cross-correlation analysis to these segments to determine the time delays between the signals from the leading and the trailing tip. Pseudo-instantaneous interfacial velocities can be calculated using the time delays and the known distance between the tips. The window was set to N_p = 5 in this study to obtain the interfacial velocity, which was most commonly recommended for hydraulic engineering applications [50,53,54]. Here, N_p equals the number of water phases considered for one segment.

2.2. Test Program

The experiments were conducted on artificial turf of different stem heights. The experimental configurations, including flow conditions and vegetation properties, are provided in Table 1. In the following configuration, the specific flow rate q_w ($m^2\ s^{-1}$), the critical flow depth $d_c = \sqrt[3]{\frac{q_w^2}{g}}$ (m), and critical flow velocity $v_c = \frac{q_w}{d_c}$ ($m\ s^{-1}$) are used to characterize the flow. The mean flow velocity u_w ($m\ s^{-1}$) was calculated from the obtained velocity measurements. The flow conditions were chosen to represent a wide range of water depths and flow velocities. Higher frequency events with normal flow depths and velocities were focused rather than extreme events. Furthermore, the chosen conditions were in the range of previous studies [14,16]. For the dike overtopping events, flow rates above 0.01 $m^2 s^{-1}$ were classified as significant [55].

Table 1. Experimental configurations tested in this study.

	Smooth	Artificial Turf		
h_i (mm)	-	15	30	40
h_{defl} (mm)	-	7–11	13–20	25–31
h_{defl}/h_i (-)	-	0.47–0.72	0.42–0.65	0.63–0.78
q_w ($m^{-2}s^{-1}$)		0.027–0.018		
d_c (m)		0.042–0.15		
Re (10^4) (-)	0.26–1.52	0.25–1.46	0.24–1.41	0.23–1.36
u_w ($m\ s^{-1}$)	2.86–5.12	1.87–4.65	2.12–4.80	1.90–4.50

Notes: h_i: initial vegetation height (mm); h_{defl}: deflected vegetation height (mm); q_w: specific flow rate (m^2s^{-1}); d_c: critical flow depth (m); Re: Reynolds number (-); u_w: mean flow velocity ($m\ s^{-1}$).

The turf used in the experiments had turf heights of 15 mm, 30 mm, and 40 mm and was fully covered with an average vegetation stem density of 1.5 cm^{-2} (see Figure 4). Artificial vegetation was used instead of natural vegetation to reduce the impact of erosion of the top layer, as was noticed in our previous laboratory studies [16]. Thus, longer measuring times were possible, providing better insights into the interaction between the top layer and overflow and the air–water flow characteristics. This study did not investigate the influence of erosion or the root system of the vegetation but the general flow characteristics and energy dissipation.

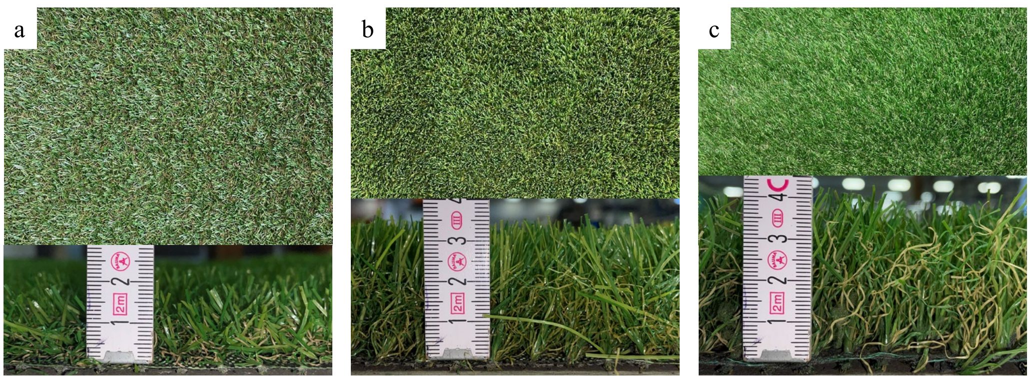

Figure 4. The top view and side view of the artificial turfs with (**a**) h_i = 15 mm, (**b**) h_i = 30 mm, and (**c**) h_i = 40 mm.

3. Results and Discussion

3.1. Inception Point and Friction Factor

In the study, the main vegetation parameters considered were the vegetation height (h_i) and the deflected vegetation height (h_{defl}) (see Figure 5). h_{defl}/h_i decreased with the increasing flow rate and velocity. With a higher bending of the turf, the layer becomes smoother, and the roughness decreases [39]. Thus, the deflected vegetation height is a significant parameter that indicates the characteristics of a turf layer. It was found that h_{defl} is primarily dependent on the flow rate (q_w), the gravitational acceleration (g), the initial vegetation height (h_i), and the Reynolds number Re, as well as the stem density (N).

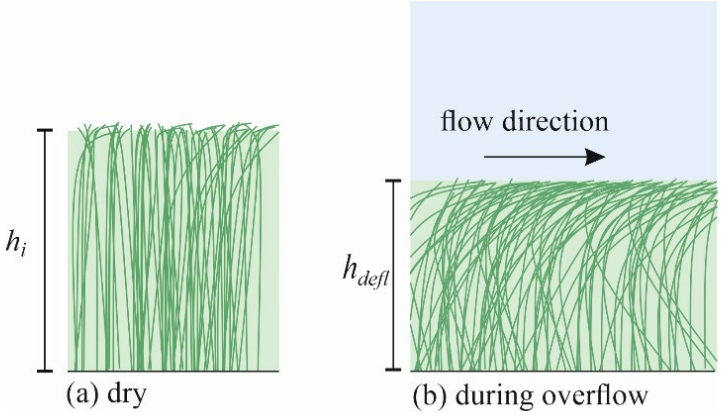

Figure 5. A schematic drawing of the initial form and the deflection of vegetation in (**a**) a dry bed and (**b**) during overflow.

The inception point (L_i (m)) marks the position where air entrainment starts. It can be observed from the top through the appearance of white water and higher turbulence on the surface. During the experiments, the inception point was visually determined using a camera. Figure 6 compares the appearance of white water and turbulences of the test cases with h_i = 15 mm and h_i = 40 mm for a flow rate of q_w = 0.063 m^{2}s^{-1}. It could be observed that the starting point of turbulences and air entrainment shifted upwards with higher vegetation height. For comparison, the point x = 0.75 m from the crest is marked with a dotted line. At that point, turbulences on the surface already appeared for the smaller vegetation height, and white water started to appear shortly after. White water was already visible at the marked point for the higher vegetation height. Thus, the influence of vegetation height can be observed.

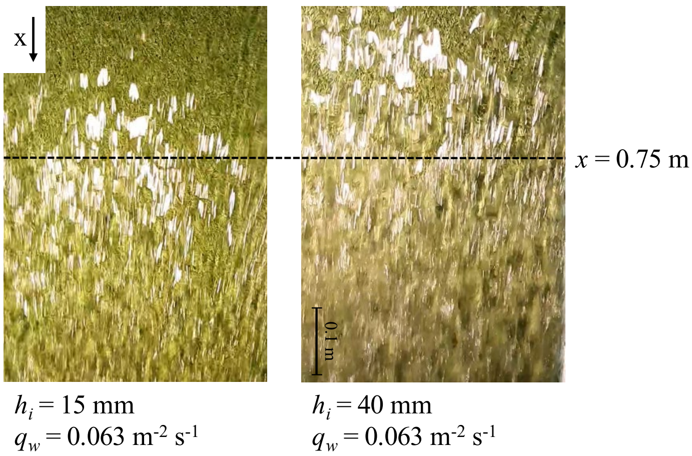

Figure 6. A comparison of the appearance of white water between h_i = 15 mm and h_i = 40 mm at q_w = 0.063 m^2/s, with x being the longitudinal distance from the crest.

The inception points in terms of the starting point of the appearance of white water are given in Figure 7 for the different cases tested. With an increasing flow rate, the inception point shifted downstream. With the increasing vegetation height, the inception point moved upwards for most cases. An exception was observed for h_i = 30 mm and flow rates of q_w = 0.027 and q_w = 0.063 m^2 s^{-1}, where the inception point was observed downstream of the inception point of h_i = 15 mm. This could be due to higher h_{def}/h in h_i = 15 mm than h_i = 30 mm, in which case, the turf surface could have resulted in a more significant shear to the flow than h_i = 30 mm, especially at lower flow depths. Thus, the flexibility and bending behavior of the three turf heights may differ. Further, uncertainty could have emerged from the method used for determining the inception point location.

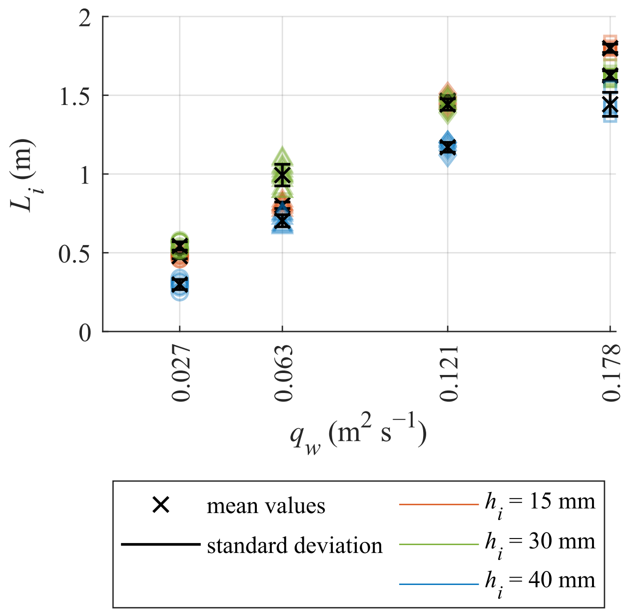

Figure 7. Inception points for the different cases as the distance from the crest with respective standard deviations.

Wood et al. (1983) [56] described the relationship between roughness height (k_s) and L_i to be dependent on q_w and α, as well as g and the Froude number (see Equations (1) and (2) by Wood et al. (1983) [56]). Based on that observation, we propose a power function to describe the relationship between h_i and L_i for the present study's data, considering h_i, g, α, and q_w (see the dotted line in Figure 8). In general, these parameters can be connected in terms of a dimensionless number, defined in this context through $\frac{g \cdot sin(\alpha) \cdot h_i^3}{q_w^2}$ (-). The consideration of k_s in the evaluation is highly sensitive to the flow velocity measurements near the boundary layer, and hence can lead to erroneous results when conductivity probes are used. Furthermore, h_i can be easily accessed in the field, and can hence simplify the design parameters. Hence, k_s was replaced with h_i for easy approximation. Figure 8 shows L_i/h_i regarding the relationship defined using h_i. The fitted equation has an R^2-value of 0.95. The equation is more accurate for lower to medium–high flow rates. Furthermore, a higher deviation was identified for h_i = 30 mm.

$$\frac{L_i}{k_s} = 7 \cdot \frac{q_w}{\sqrt{g \cdot \sin(\alpha) \cdot k_s^3}} \quad \left(0 < \frac{q_w}{\sqrt{g \cdot \sin(\alpha) \cdot k_s^3}} < 10 - 30\right) \tag{1}$$

$$\frac{L_i}{k_s} = 15.5 \cdot \left[\frac{q_w}{\sqrt{g \cdot \sin(\alpha) \cdot k_s^3}}\right]^{0.7} \quad \left(10 - 30 < \frac{q_w}{\sqrt{g \cdot \sin(\alpha) \cdot k_s^3}} < 10^6\right) \tag{2}$$

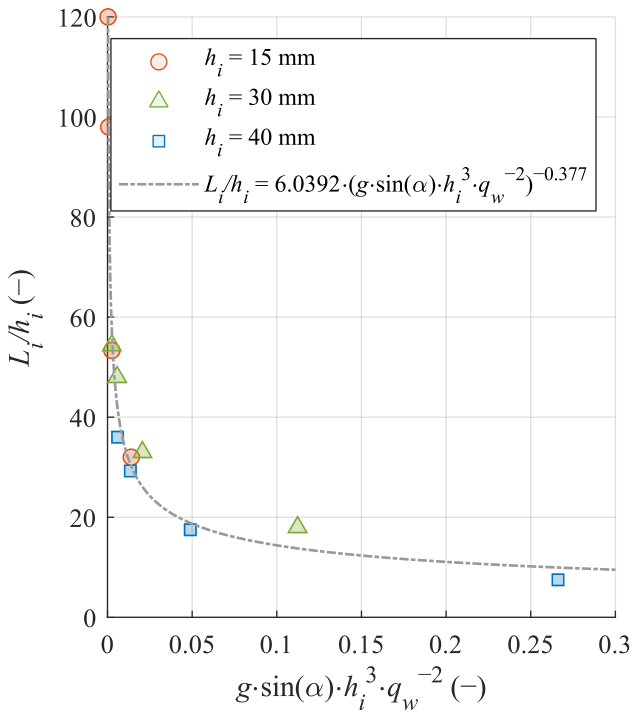

Figure 8. The relation of L_i/h_i versus the dimensionless parameter $\frac{g \cdot sin(\alpha) \cdot h_i^3}{q_w^2}$, illustrating the influence of gravity, the slope angle, the flow height, and specific discharge on the inception point through a fitted power function.

The general observation that the inception point shifts upwards for lower flow rates and higher vegetation heights is in alignment with other studies [14,57,58].

The equivalent Darcy–Weisbach friction factors f_e (-) were calculated from Equation (3) based on the air–water flow measurements as a mean over the entire chute ($1.9 \leq x \leq 4.9$):

$$f_e = \frac{8 \cdot g \cdot S_f \cdot \left(\int_0^{y_{90}} (1 - C) \cdot dy\right)^3}{q_w^2} \quad (3)$$

where S_f is the friction slope, which considers the slope and the change in flow depth over the entire spillway.

The friction factors are presented in Figure 9, which includes the comparison with natural vegetation. The friction factors for artificial turf increased with the increasing vegetation height and lower flow rate, and were in the range of $0.08 \leq f_e \leq 2.4$. The high value of 2.4 was calculated for h_i = 40 mm and q_w = 0.027 m^2 s^{-1}. The flow development on top of the artificial turf might have influenced the calculation. Generally, high values were calculated for the lowest flow rate for all turf heights. For h_i = 15 mm, the lowest friction factors were obtained. Even though the artificial turf heights were lower than the natural vegetation heights in Scheres et al. (2020) [16], similar friction factors were observed, possibly due to the different flexibility of natural vegetation and artificial turf. Furthermore, the values for natural vegetation were within a limited range, while for artificial turf, a wider range was observed. This could be due to bending behavior and flexibility. The artificial turf showed different deflection levels for the different flow rates. Although comparable friction factors for artificial and natural turf were obtained, the vegetation height differed. Nevertheless, Figure 9 clarifies that an increase in the vegetation height and a decrease in the flow rate increased friction, and hence, the inception point moved upstream.

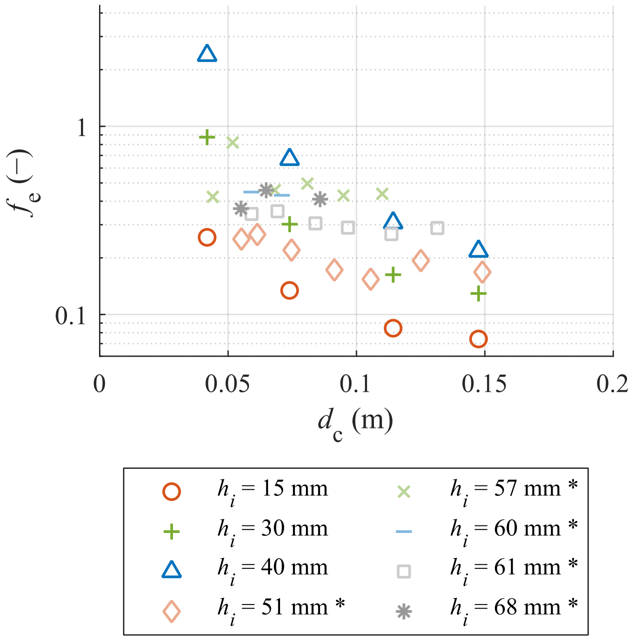

Figure 9. The Darcy–Weisbach friction factor f_e for different flow conditions and vegetation heights in comparison to Scheres et al. (2020) [16]'s natural vegetation data (data marked with * refers to Scheres et al. (2020) [16]).

3.2. Air Concentration

From the conductivity probe's signal, the air concentration can be derived from the phase changes as described above. The mean concentration is calculated from the following:

$$C_{mean} = \frac{1}{y_{90}} \int_0^{y_{90}} C\, dy \tag{4}$$

where C is the air concentration (-), and y_{90} is the flow depth (m), at which C = 0.9. The clear-water depth d_{eq} (m) can be calculated through Equation (5):

$$d_{eq} = (1 - C_{mean}) \cdot y_{90} \tag{5}$$

Three repetitions were conducted for each test case. In general, the air concentrations derived from the signal of the repetitions were in good agreement. The standard deviation was higher with a lower air concentration. Overall, an average standard deviation of 0.01 (-) was found for all the cases tested, indicating good repeatability of the conducted tests.

Figure 10 shows the air concentration as a function of the dimensionless flow depth y/y_{90} for the different test cases. It could be observed that for higher vegetation heights, a higher air profile over the flow depth was developed. The air concentration at x = 1.9 m was the lowest for all cases, as the inception points were only slightly before that measuring point. Air entrainment without vegetation during the test case only occurred at the surface of the flow.

A changing air concentration along the length of the chute was observed, especially for higher vegetation heights and lower flow rates. The mean air concentration slightly increased at the second measuring position and decreased afterwards. This could be due to the influence between bending and flow resistance, respectively, and the longitudinal velocity distribution. Scheres et al. (2020) [16] described a similar phenomenon during the experiments with the natural vegetation turf.

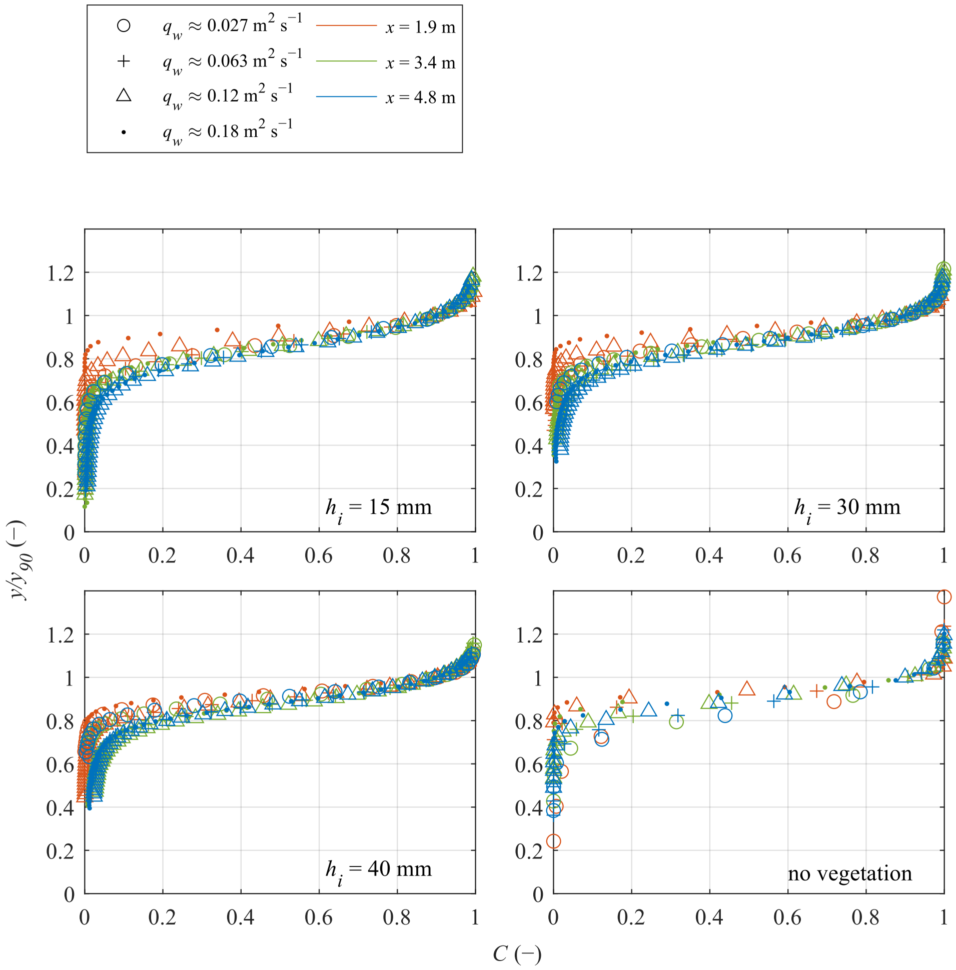

Figure 10. The distribution of air concentration C on vegetated and smooth chutes as a function of the dimensionless flow depth y/y_{90} for different flow rates at the three measuring points (x) for varying vegetation heights.

In general, it can be observed that the distribution follows an inverse sigmoid function in the following form:

$\frac{y}{y_{90}} = -a \cdot \left(\ln\left(\frac{1}{C} - 1\right) - b\right)$, where a and b are constants depending on the bottom layer, x, L_i, and q_w, ranging between $0.021 < a < 0.092$ and $8.8 < b < 45.52$. For the data collected in this study, R^2 ranges between $0.9183 < R^2 < 0.9995$, and the root mean square error (*RMSE*) ranges between $0.0021 < RMSE < 0.086$. The function generally fits better for the smaller flow rates (q_w = 0.027 m^2 s^{-1}) and the first two measuring positions (x = 1.9 m and 3.4 m). R^2 decreases for the last measuring position and higher flow rates (q_w = 0.12 m^2 s^{-1} and q_w = 0.18 m^2 s^{-1}).

The mean air concentration for the vegetated layers ranges from 0.06 (q_w = 0.18 m^2 s^{-1} and h_i = 15 mm) to 0.18 (q_w = 0.12 m^2 s^{-1} and h_i = 15 mm). Figure 11 shows the normalized distance from the inception point and the mean air concentration. The figure shows that the mean air concentration increases with increasing distance from the inception point for higher vegetation heights. With the further increase in flow length, C_{mean} attains a constant value, agreeing with Cui et al. (2022) [32]. Figure 11 also shows a comparison with data from Bai et al. (2022) [14]'s study. In Bai et al. (2022) [14]'s study, artificial turf layers with heights of h_i = 15 mm and 25 mm were used on a spillway with a slope angle of 21.8°. The data follow a similar trend, showing an increase in air concentration with the increasing distance from the crest and for higher vegetation heights. However, it is to be recognized that the tested slope in Bai et al. (2022) is steeper, and an increase in mean air concentration can be seen compared to the present study. In addition, the present study also investigated lower flow rates, which explains the lower values.

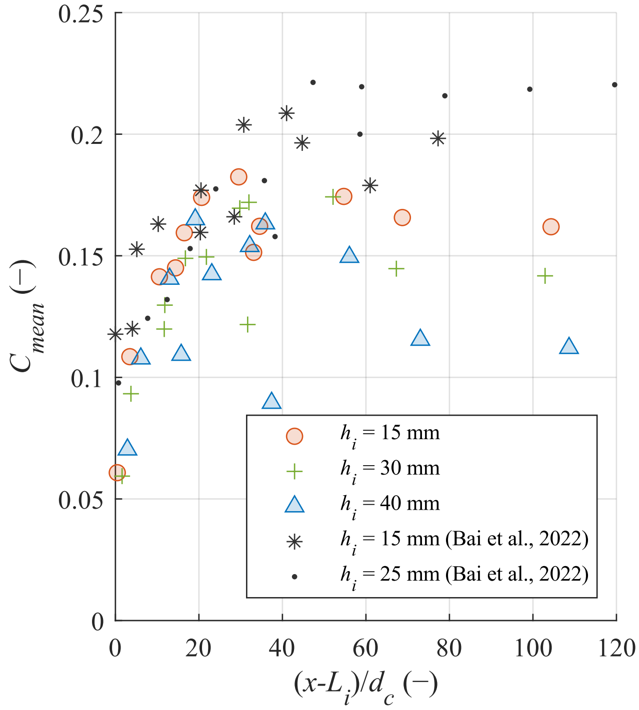

Figure 11. The mean air concentration C_{mean} over a normalized distance from the inception points for the present study's vegetation heights and a comparison to Bai et al. (2022)'s data [14].

The mean air concentration C_{mean} at a particular point x can be described through a power function depending on the inception point (L_i) and the critical flow depth (d_c), as well as the vegetation height (h_i), the slope angle ($\sin(\alpha)$), and the flow rate (q_w). The fitted function (Equation (6) is suitable for $x > L_i$, and q_w, d_c, h_i, and $\sin(\alpha) > 0$, respectively. The *RMSE* amounts to 0.053, and the R^2 is 0.83. The function was also applied to the data considering the artificial turf in Bai et al. (2022) [14]'s study. The quality of the fit is presented in Figure 12 as a comparison of the measured and calculated mean air concentration C_{mean} based on Equation (6). The equation generally fits better for lower flow rates and with a higher distance from the crest. Furthermore, the equation provided a decent estimate for h_i = 15 mm and h_i = 25 mm from Bai et al. (2022) [14]'s data, proving the adequacy of the proposed equation for slope between 1:3 and 1:2.5.

$$C_{mean} = 0.0434 \cdot \left[\frac{x - L_i}{d_c}\right]^{0.237} \cdot \left[\frac{q_w^2}{g \cdot sin\alpha \cdot h_i^3}\right]^{0.085} \quad (6)$$

Differences in the vertical position of specific air concentrations (10% and 90%) were observed for the different top layers. Figure 13 compares y_{10} and y_{90} over the longitudinal distance of the chute, where y_{10} and y_{90} are the flow depths at which C = 0.1 and C = 0.9, respectively. While these two values were close to each other with the smooth bottom layer from PVC, a different distribution was observed for the vegetated layers. For higher h_i and q_w, y_{10} is near the free surface at the first measuring position (i.e., close to the inception point) and moved closer to the bottom with increasing distance from the crest. This implies that the air entrainment increased over the longitudinal distance. For q_w = 0.027 m^2 s^{-1}, y_{10} amounted to similar values at the different measuring positions, meaning the inception point was further upstream, and the aeration process has already fully developed to a certain degree, at which the concentration in the flow depth remains almost equal. The data observed that the vegetated turf layer influenced y_{90}. While y_{90} amounted to 7 to 42 mm for the PVC layer, it increased when testing with the artificial turf layer. It was also observed that for the PVC layer, the value decreased with the increasing distance from the crest for the highest flow rate by 12%, with an increase of 3% for h_i = 15 mm and a slight decrease by 4% for h_i = 30 and 40 mm which could be observed along the length of the chute.

However, this comparison also shows an increase due to the turf height. For lower flow rates, y_{90} was rather equal (h_i = 30 and 40 mm) or increased slightly (h_i = 15 mm and PVC) along the spillway. Since y is defined from the bottom, the turf height adds to the water depth as well. Still, it shows that, especially for higher turf heights, y_{90} remained at an equal level, indicating close to fully developed aeration.

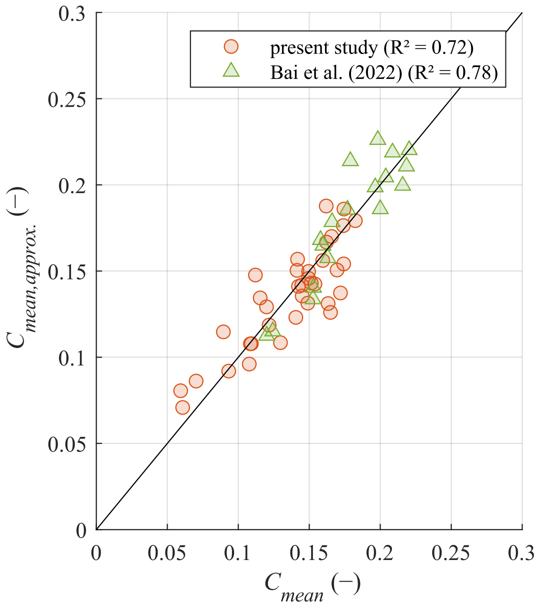

Figure 12. The quality of the fitted function (Equation (6)) as a comparison of actual data in x- and the approximated data in the y-direction for the present study and Bai et al. (2022) [14].

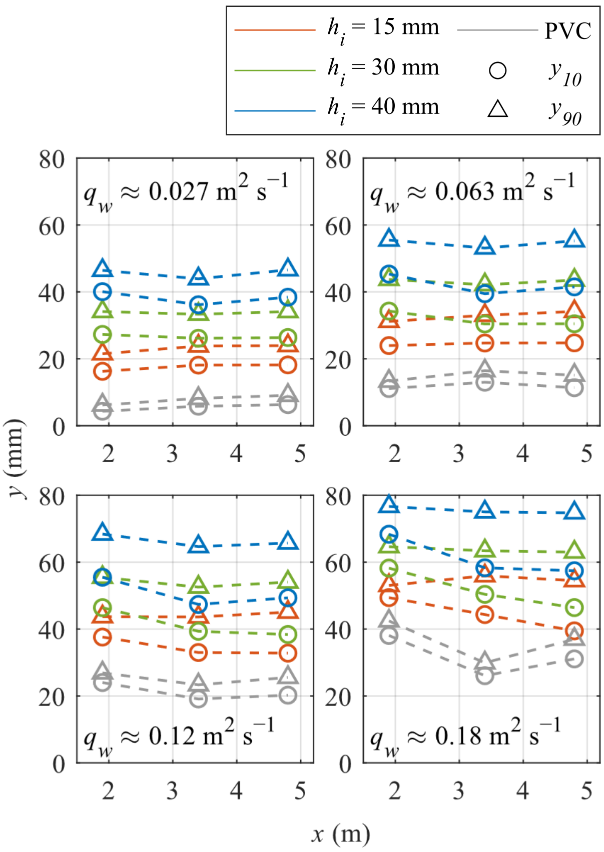

Figure 13. y_{90} and y_{10} over the flow length of the spillway for different flow rates and bottom layers.

These findings highlight the significant impact of the top layer on air concentration distribution along the chute, with vegetated layers demonstrating a higher variability and increased air entrainment compared to the PVC layer. This suggests that the vegetation height significantly influences turbulence and mixing, affecting the overall aeration dynamics more substantially than smoother, non-vegetated surfaces.

3.3. Bubble Count Frequency

The bubble count frequency F gives information on the number of bubbles crossing the sensor per second. From that, it can be derived how the air entrainment developed over the depth and the length of the chute, and this provides information on the fragmentation of air–water flow [59]. Understanding the bubble count frequency is essential since turbulence intensities can be derived from bubble count rates, which provide information on the point of interest for erosion and local pressure on the embankment. Further, such measurements are necessary to accurately assess the flow behavior since air entrainment can reduce the density and viscosity of the flow, thereby reducing hydraulic pressure, but can also increase the potential for cavitation. In addition, bubble count rates provide insights into the degree of air entrainment and energy dissipation.

Figure 14 shows the bubble count frequency in terms of a dimensionless number as a function of bubble frequency F (s^{-1}), critical flow depth d_c (m), and critical flow velocity v_c (m s^{-1}) over the flow depth y/y_{90} for the flow rates of q_w = 0.027 m^2 s^{-1} and 0.12 m^2 s^{-1}. It can be observed that F increased with the increasing flow rate, the increasing vegetation height, and the increasing distance from the crest. Furthermore, Figure 14 indicates that the bubbles were more present near the bottom layer for the increasing distance from the crest, and F grew gradually over the flow depth.

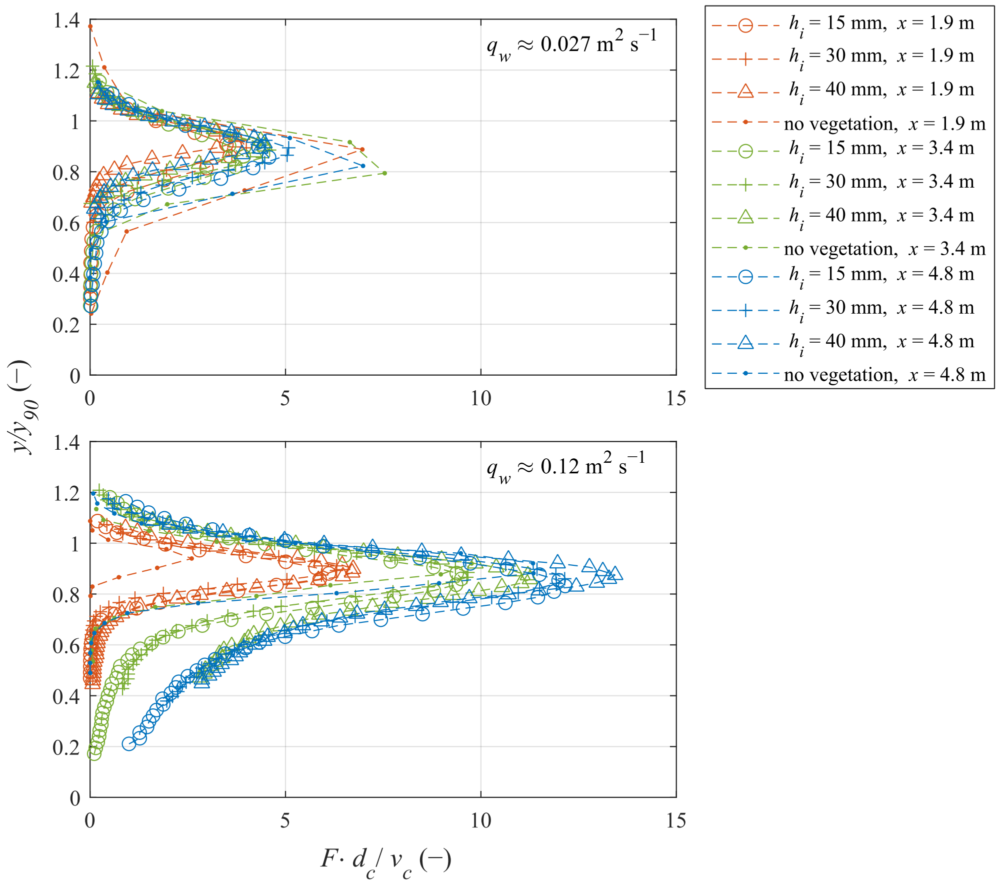

Figure 14. A comparison of the bubble count frequency as a function of critical flow depth and critical flow velocity for different flow rates and different vegetation heights over the flow depth y/y_{90}.

The maximum bubble count rates F_{max} for the turf layers were observed for a flow depth y/y_{90} = 0.88 (total range: 0.83 < y/y_{90} < 0.95), which is slightly higher than what was found in Scheres et al. (2020) [16], who observed F_{max} at y/y_{90} = 0.75 with natural vegetation. F_{max} was observed at air concentrations of C = 0.50 (total range: 0.44 < C < 0.61), which agrees with previous studies on self-aerated flows [16,60]. Bai et al. (2018) [60] suggested a correlation between bubble count and turbulence intensity and found an increase in both parameters from the bottom of the flow. The maximum bubble count rate F_{max} = 124 Hz was observed for q_w = 0.12 m^2 s^{-1} and a turf layer with h_i = 40 mm at x = 4.8 m. In general, F_{max} increased with the increasing flow rate until q_w = 0.12 m^2 s^{-1} and decreased slightly for the highest flow rate of q_w = 0.18 m^2 s^{-1}, which could be due to the shift of the inception points and thus, the air concentration and the formation of bubbles along the chute. Figure 15 shows the longitudinal distribution of $F_{max,}$ taking the shift due to the inception point into consideration. It indicates that F_{max} remains almost equal for a lower q_w and shows a steeper bubble increase for higher flow rates, which implies that the equilibrium has not yet reached the last measuring points. Thus, a higher F_{max} was expected further downstream x = 4.8 m for q_w = 0.18 m^{2}s^{-1}.

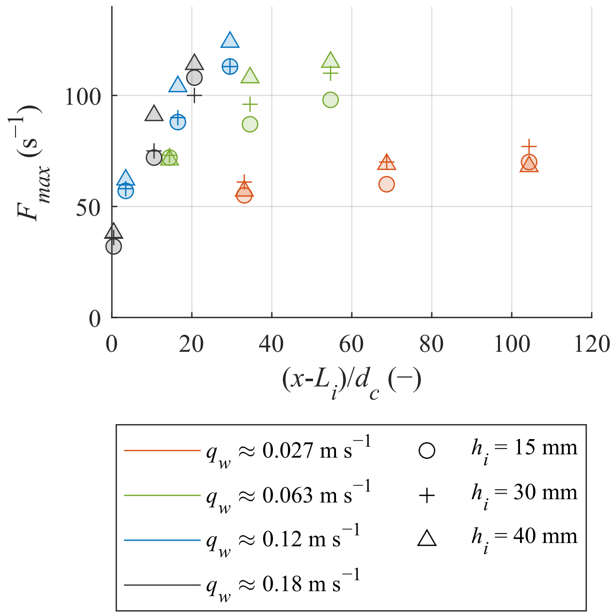

Figure 15. The distribution of the maximum bubble frequency F_{max} over the normalized distance $(x\text{-}L_i)/d_c$.

Higher F values of up to F = 266 Hz were observed in Scheres et al. (2020) [16], which could be explained by the higher vegetation heights and higher flow velocity tested in their experiments. However, the trend of variation of bubble frequency agrees with the general observation that higher vegetation heights induce higher air entrainment, respectively higher bubble number in the flow. Still, the grass-dominated mixture, which comes closest to the artificial turf used in this study, showed a similar distribution of the bubble count. The increasing bubble count rate F, with increasing flow rates and increasing distance from the crest, was also observed in other studies on air–water flows over vegetated spillways [14,16].

3.4. Energy Dissipation and Flow Velocity

To reduce damage to the embankment, energy dissipation is of importance. Energy dissipation due to vegetation helps minimize the erosive capacity of the overflow, and hence, it is necessary to estimate the magnitude of energy dissipation. For estimating the energy dissipation capacity, the residual energy height, H_{res}, can provide information. H_{res} was calculated for the downstream end (x = 4.8 m from the crest) using Equation (7):

$$H_{res} = \int_0^{y_{90}} (1-C)\cos\alpha\, dy + \frac{{q_w}^2}{2\cdot g\cdot \left(\int_0^{y_{90}} (1-C)\cdot dy\right)^2} \quad (7)$$

where cos α is the angle of the slope.

Figure 16 shows the relation between the residual energy height of the vegetated and smooth slopes at the end of the chute (x = 4.8 m). H_{res} decreased by up to 90 % for lower flow rates, with h_i = 40 mm compared to PVC. With the increasing flow rate, the energy dissipation reduction on vegetated compared to smooth spillways was lowest and amounted to about 40–70%, possibly due to higher bending with increasing flow velocity and lower resistance (or friction factor). A comparison to the friction factors f_e obtained showed that a lower f_e resulted in higher residual energies H_{res}, which supports the observation. However, it shows that a vegetated slope can dissipate more energy for lower flow rates and higher turf heights than smooth slopes. The dashed lines show the relation between vegetated and stepped spillways using the approximation of $H_{res,stepped}$ = 4.6 d_c for slope angles between 15.9 and 21.8°, as proposed by Chanson and Felder (2010) [61]. If the product of $H_{res,veg}$ and $H_{res,stepped}$ is below one, it is indicated that $H_{res,stepped}$ is greater; thus, there is less energy dissipation during the overflow of the stepped spillway. From the figure, it can be seen that $H_{\mathrm{res,veg}}/H_{\mathrm{res,stepped}}$ < 1 for h_i = 30 and 40 mm for d_c < 0.15 m. Thus, for critical flow depths below 0.15 m, energy dissipation is higher on vegetated spillways. However, with an increasing flow rate, the relationship possibly exceeds 1. Furthermore, for lower vegetation heights on the spillway, $H_{res,veg}/H_{res,stepped}$ reaches 1 for critical flow depths below 0.1 m. This shows that the energy dissipation capability of vegetated spillways with higher vegetation heights is comparable to stepped spillways, while stepped spillways perform better for higher flow rates.

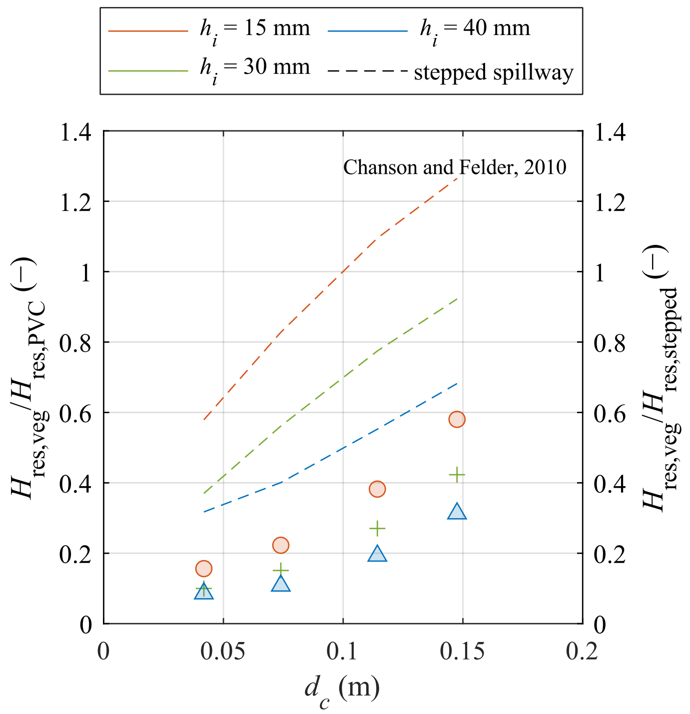

Figure 16. The relation between residual energy $H_{res,veg}$ and d_c at the downstream end of the chute for different vegetated layers compared to the PVC bottom layer and a comparison to stepped spillways (dashed lines) [61].

This study obtained dimensionless values in the range of 1.45 $\leq H_{res}/d_c \leq$ 5.82. For natural vegetation, values between 1.77 and 3.18 were found by Scheres et al. (2020) [16], which is comparable to the data obtained in the present study. Furthermore, the general observation of higher residual energies with a lower vegetation height aligns with the previous study [16]. The present tests did not induce erosion or sediment transport since the experiments were conducted with artificial turf. If erosion or bare spots are considered, they are likely to increase energy dissipation due to undulations that are created during successive experimental runs. On the other hand, erosion can increase the risk of failures, which should be avoided in order to provide stability.

A critical parameter for spillway design is the flow velocity along the chute. Figure 17 shows the velocity profiles over the normalized flow depth for various flow rates and bottom layers over the chute length (x = 1.9 m, 3.4 m, and 4.8 m from the crest). The velocities were derived from the bubble velocity calculated using the signal from the conductivity probes. The mean velocities are presented in the figure. For the PVC layer, the flow velocity increased in a longitudinal direction over the spillway when comparing the data at x = 1.9 and x = 4.8 m. At x = 1.9 m, the flow velocity was lowest for h_i = 15 mm, whereas at x = 4.8 m, the lowest flow velocity was observed for h_i = 40 mm, indicating a higher reduction and the influence of vegetation height. Specifically, the velocity v_{90} (the velocity at which C = 0.9) increased by 4–15% over the flow length for the PVC bottom layer. In general, v was lower for the turf layers, while v_{90} also decreased, especially for h_i = 30 and 40 mm, by up to 13% for q_w = 0.027 and 0.063 m^2 s^{-1} over the flow length. An increase in v over the flow length could be observed for the turf with h_i = 15 mm at every flow rate. However, the flow velocity for the vegetated bottom with h_i = 15 mm was still lower than for the PVC bottom. The highest reduction in v_{90} compared to PVC of 43% was achieved with the vegetated turf h_i = 40 mm at a flow rate of q_w = 0.027 m^2 s^{-1}. Lower reduction rates were observed for higher flow rates. The velocity measurements showed standard deviations (*std*) ranging between 0.035 m s^{-1} < *std* < 0.82 m s^{-1}. Notably, higher standard deviations were observed at x = 1.9 m for higher flow rates, likely due to the lower air concentration in the flow at this position.

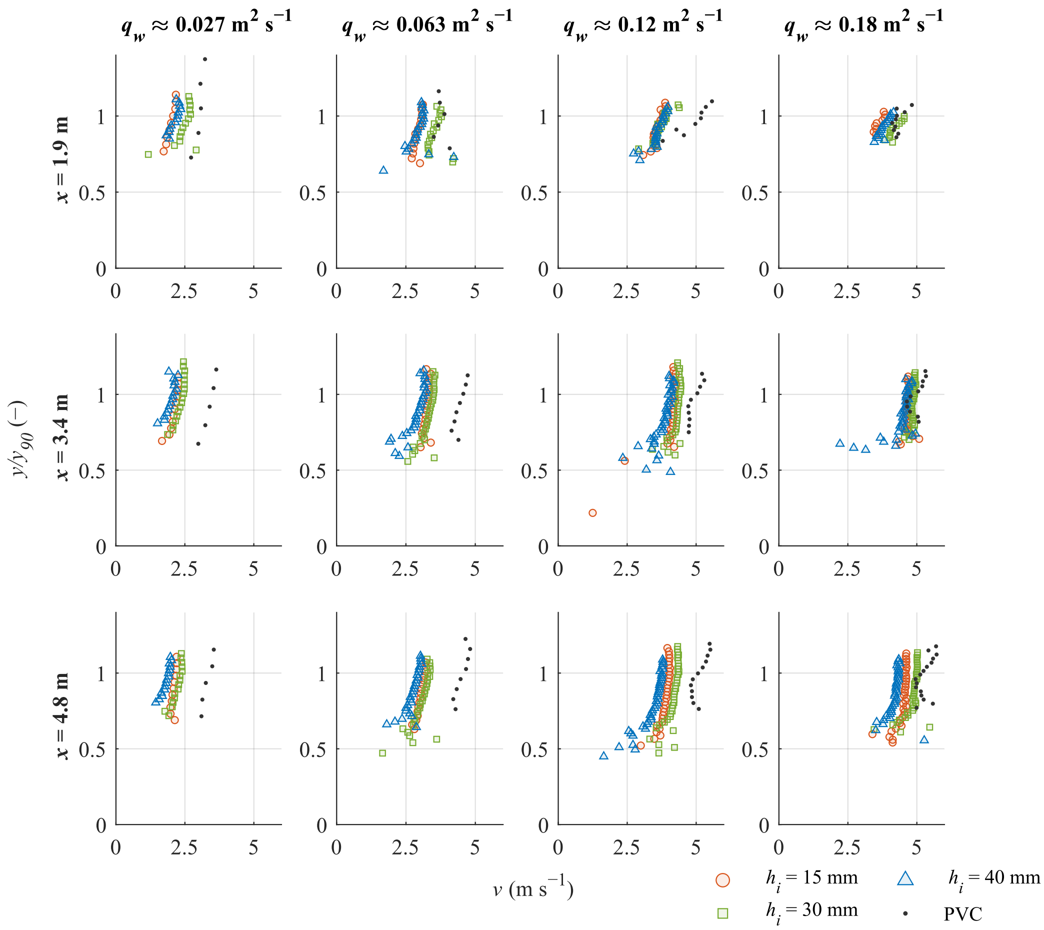

Figure 17. A comparison of the flow velocity v over the normalized flow depth y/y_{90} at x = 1.9 m, 3.4 m, and 4.8 m for different flow rates and bottom layers.

It should be noted that the flow velocity of an aerated flow is underestimated if the water depth (y_{90}) is considered instead of the equivalent water depth (d_{eq}). In general, the mean flow velocity (u_w) was usually 6–22% lower when calculated from y_{90} compared to d_{eq}. This shows how crucial it is to understand and know air–water flow and air concentrations.

Table 2 summarizes the key findings of the conducted tests for the investigated turf heights as a range of parameters. The study found that higher vegetation heights resulted in higher friction factors. With higher friction factors, the inception point moved further upstream. Thus, more aeration was found, which is also supported by bubble count rates. A higher energy dissipation for greater vegetation heights was indicated.

Table 2. A summary of the key parameter for the investigated turf heights.

	h_i = 15 mm	h_i = 30 mm	h_i = 40 mm
u_w (m s^{-1})	1.87–4.67	2.12–4.80	1.90–4.50
L_i (m)	0.48–1.80	0.54–1.63	0.3–1.44
y_{90} (m)	0.021–0.053	0.034–0.065	0.046–0.077
d_{eq} (m)	0.018–0.050	0.029–0.061	0.028–0.071
f_e (-)	0.08–0.26	0.13–0.88	0.22–2.38
C_{mean} (-)	0.061–0.18	0.059–0.17	0.07–0.16
H_{res} (m)	0.11–0.86	0.071–0.63	0.061–0.46
F_{max} (Hz)	32–113	36–113	38–124

4. Conclusions and Future Outlook

The study aimed to systematically investigate the influence of different vegetation heights on air–water flow during the overflow of vegetated spillways. A bottom layer made of PVC and artificial turf layers of 15, 30, and 40 mm vegetation heights were used in experiments on a 1:3 sloped embankment in a 1:1 scale. During the experiments, the flow rate varied between q_w = 0.027 and q_w = 0.18 m^{2}s^{-1}. The bending of the vegetation and the inception point were monitored using a camera. The air concentration in the flow was measured with double-tip conductivity probes. The raw data were analyzed using the AWCC method, and the flow velocity was derived.

The experimental results showed the typical air concentration profiles over the chute's length and the flow depth, with increasing aeration closer to the surface and the end of the spillway. An increasing air entrainment effect was observed for higher vegetation heights due to higher flow friction. The air inception point moved downstream with higher flow rates and upstream with higher vegetation heights. A more significant air profile over the flow depth was found for higher vegetation heights. In general, the air concentration can be described as a variation of the sigmoid function, with the vegetation height and flow rate as influencing factors. The mean air concentration at a specific position was found to be primarily dependent on the vegetation height, the position of the inception point, the flow rate, and gravitational acceleration. Higher bubble count frequencies were obtained for higher vegetation heights and flow rates at the end of the chute. With higher vegetation heights, more bubbles were observed. Regarding energy dissipation along the chute, the highest vegetation layer showed the most significant energy dissipation for lower flow rates. A lower energy dissipation was observed for high flow rates. The flow velocities mainly decreased over the chute's length with vegetated turf layers. All turf lengths showed a lower flow velocity than the PVC layer's flow velocity. The highest flow velocity reduction over the chute's length was observed for the highest turf height.

The present study results were based on experiments with artificial turf of different heights for particular flow conditions. The results should be seen as the first guidance on the effect of vegetation, providing information on flow velocities, aeration, and bubble count rates, from which design parameters could be derived. The study highlights the importance of the consideration of air concentration as it impacts the estimation of flow velocities.

The results show that nature-based solutions such as the vegetated spillways have a comparable ability to dissipate energy to conventional structures, and thus, present an alternative strategy with advantages such as ecological and biodiversity enhancement. Future studies should focus on validations using natural turf, which comes with different flexibility than artificial turf and has a higher possibility of erosion of the top layer and sediment transport, thereby carrying uncertainties and impacting the flow behavior and energy dissipation. Furthermore, a flow development above the turf was observed rather than within the individual stems, which could be different from natural vegetation. The comparison with natural vegetation showed that energy dissipation and friction factors were in the same value range for different vegetation heights. Thus, flexibility and bending behaviors are critical, and a transfer of the results based on only vegetation height is limited. In addition, a systematic investigation of the vegetation density of the turf layer could give new insights into the influence of vegetation properties on overflow and air entrainment. This study investigated lower flow depths, which are common during normal conditions, such as mild flood events. In future studies, higher flow rates representing severe flow events, such as during intense flood events, could be investigated to understand the potential of vegetated spillways with increasing flow rates.

Furthermore, the manual vertical shift of the sensors may represent a source of errors in this study due to human error. In the present study, this was reduced by frequently checking the vertical shift of the sensor with a measurement scale with the least count of one mm. Thus, this prevented adjustment in less than one mm increments. The measuring steps were, therefore, in mm, and the bar was used to shift as accurately as possible. An automated vertical shift is recommended for more precise measurements for future studies.

Author Contributions: Conceptualization, A.M.; methodology, A.M.; validation, A.M.; formal analysis, A.M.; investigation, A.M.; data curation, A.M.; writing—original draft preparation, A.M.; writing—review and editing, S.H.; visualization, A.M. and S.H.; supervision, S.H. All authors have read and agreed to the published version of the manuscript.

Funding: This research was funded by the German Research Foundation (DFG), funding code: SCHU 1054/24-1.

Data Availability Statement: Data are available on request.

Acknowledgments: The authors thank the technical staff (Kristian Brodersen, Arne Harz, Lars König, Peter Kläser, and Jannik Ulbrich) and student assistant Kathrin Mikosch for their help with the model tests.

Conflicts of Interest: The authors declare no conflicts of interest. The funders had no role in the design of the study; in the collection, analyses, or interpretation of data; in the writing of the manuscript; or in the decision to publish the results.

References

1. Buck, W. Konzeptionelle Überlegungen und Vorschläge zur Gewährleistung angemessener Hochwassersicherheiten bei wasserwirtschaftlichen Anlagen. In *Risiken bei der Bemessung und Bewirtschaftung von Fließgewässern und Stauanlagen: Dresdner Wasserbauliche Mitteilungen*; Institut für Wasserbau und technische Hydromechanik, Technische Universität Dresden: Dresden, Germany, 2004; Volume 27.
2. Ozueigbo, O.; Agunwamba, J.C. New Equations for Energy Dissipation down a Stepped Spillway. *J. Eng. Res. Rep.* **2022**, *23*, 1–14. [CrossRef]
3. Degoutte, G.; Tourment, R. (Eds.) *Spillways on River Levees*; Quae: Versailles, France, 2021.
4. Mickovski, S.B.; Gonzalez-Ollauri, A.; Sorolla, A.; Löchner, A.; Emmanuel, R. A case history of co-design and co-deployment of a nature-based solution (NbS) against erosion and slope instability. *Ecol. Eng.* **2024**, *209*, 107406. [CrossRef]
5. Sinha, V.R.; Bimson, K. *Nature-Based Solutions in the Ganges Brahmaputra Meghna (GBM) River Basin: Case Studies and Lessons Learned*; Sinha, V.R., Bimson, K., Eds.; IUCN Asia Regional Office (ARO): Bangkok, Thailand, 2021. Available online: https://iucn.org/sites/default/files/content/documents/2021/nbs_in_the_gbm_river_basin_case_studies_and_lessons_learned_iucn_final_2.pdf (accessed on 24 October 2024).
6. Jakubínský, J.; Prokopová, M.; Raška, P.; Salvati, L.; Bezak, N.; Cudlín, O.; Cudlín, P.; Purkyt, J.; Vezza, P.; Camporeale, C.; et al. Managing floodplains using nature-based solutions to support multiple ecosystem functions and services. *WIREs Water* **2021**, *8*, e1545. [CrossRef]
7. van der Meulen, F.; IJff, S.; van Zetten, R. Nature-based solutions for coastal adaptation management, concepts and scope, an overview. *Nord. J. Bot.* **2023**, *2023*, e03290. [CrossRef]
8. Pontee, N.; Narayan, S.; Beck, M.W.; Hosking, A.H. Nature-based solutions: Lessons from around the world. *Marit. Eng. J.* **2016**, *169*, 29–36. [CrossRef]

9. Griscom, B.W.; Adams, J.; Ellis, P.W.; Houghton, R.A.; Lomax, G.; Miteva, D.A.; Schlesinger, W.H.; Shoch, D.; Siikamäki, J.V.; Smith, P.; et al. Natural climate solutions. *Proc. Natl. Acad. Sci. USA* **2017**, *114*, 11645–11650. [CrossRef]
10. Oral, H.V.; Carvalho, P.; Gajewska, M.; Ursino, N.; Masi, F.; van Hullebusch, E.D.; Kazak, J.K.; Exposito, A.; Cipolletta, G.; Andersen, T.R.; et al. A review of nature-based solutions for urban water management in European circular cities: A critical assessment based on case studies and literature. *Blue Green Syst.* **2020**, *2*, 112–136. [CrossRef]
11. Huang, Y.; Tian, Z.; Ke, Q.; Liu, J.; Irannezhad, M.; Fan, D.; Hou, M.; Sun, L. Nature-based solutions for urban pluvial flood risk management. *WIREs Water* **2020**, *7*, e1421. [CrossRef]
12. Schüttrumpf, H.; Oumeraci, H. Layer thicknesses and velocities of wave overtopping flow at seadikes. *Coast. Eng.* **2005**, *52*, 473–495. [CrossRef]
13. Wang, H.; Bai, Z.; Bai, R.; Liu, S. Self-Aeration of Supercritical Water Flow Rushing Down Artificial Vegetated Stepped Chutes. *Water Resour. Res.* **2022**, *58*, e2021WR031719. [CrossRef]
14. Bai, R.; Bai, Z.; Wang, H.; Liu, S. Air-Water Mixing in Vegetated Supercritical Flow: Effects of Vegetation Roughness and Water Temperature on Flow Self-Aeration. *Water Resour. Res.* **2022**, *58*, e2021WR031692. [CrossRef]
15. Felder, S. Air-Water Flow Properties on Stepped Spillways for Embankment Dams: Aeration, Energy Dissipation and Turbulence on Uniform, Non-Uniform and Pooled Stepped Chutes. Ph.D. Thesis, University of Queensland, Brisbane, Australia, 2013.
16. Scheres, B.; Schüttrumpf, H.; Felder, S. Flow Resistance and Energy Dissipation in Supercritical Air-Water Flows Down Vegetated Chutes. *Water Resour. Res.* **2020**, *56*, e2019WR026686. [CrossRef]
17. Chanson, H. Self-Aerated Flows on Chutes and Spillways. *J. Hydraul. Eng.* **1993**, *119*, 220–243. [CrossRef]
18. Chanson, H. Design of weirs and spillways. In *Hydraulics of Open Channel Flow*; Elsevier: Amsterdam, The Netherlands, 2004; pp. 391–430.
19. Hunt, S.L.; Kadavy, K.C. Inception Point for Embankment Dam Stepped Spillways. *J. Hydraul. Eng.* **2013**, *139*, 60–64. [CrossRef]
20. Jalili Ghazizadeh, M.; Zarrati, A.R.; Ostad Mirza Tehrani, M.J. Numerical Modeling of Self-Aeration in High-Speed Flows over Smooth Chute Spillways. *J. Hydraul. Eng.* **2023**, *149*, 04022042. [CrossRef]
21. Zhang, G.; Chanson, H. Self-aeration in the rapidly- and gradually-varying flow regions of steep smooth and stepped spillways. *Environ. Fluid Mech.* **2017**, *17*, 27–46. [CrossRef]
22. Chanson, H. Turbulent air–water flows in hydraulic structures: Dynamic similarity and scale effects. *Environ. Fluid Mech.* **2009**, *9*, 125–142. [CrossRef]
23. Chanson, H. Air Entrainment in steep chute flows. In *Air Bubble Entrainment in Free-Surface Turbulent Shear Flows*; Chapter 10; Academic Press: Cambridge, MA, USA, 1996; pp. 110–132.
24. Hunt, S.L.; Kadavy, K.C. Inception Point Relationship for Flat-Sloped Stepped Spillways. *J. Hydraul. Eng.* **2011**, *137*, 262–266. [CrossRef]
25. Severi, A. Aeration performance and flow resistance in high-velocity flows overmoderately sloped spillways with micro-rough bed. Ph.D. Thesis, UNSW Syndey, Sydney, Australia, 2018.
26. Wood, I.R. (Ed.) *Air Entrainment in Free-Surface Flows*; Balkema: Rotterdam, The Netherlands, 1991.
27. Wei, W.; Deng, J. Free surface aeration and development dependence in chute flows. *Sci. Rep.* **2022**, *12*, 1477. [CrossRef]
28. Straub, L.G.; Anderson, A.G. Experiments on Self-Aerated Flow in Open Channels. *J. Hydr. Div.* **1958**, *84*, 1–35. [CrossRef]
29. Bai, Z.; Wang, H.; Bai, R. Fully developed self-aerated flow in steep chute with various bottom roughness. *Phys. Fluids* **2024**, *36*, 073322. [CrossRef]
30. Felder, S.; Chanson, H. Aeration, Flow Instabilities, and Residual Energy on Pooled Stepped Spillways of Embankment Dams. *J. Irrig. Drain Eng.* **2013**, *139*, 880–887. [CrossRef]
31. Thorwarth, J. Hydraulisches Verhalten von Treppengerinnen mit eingetieften Stufen—Selbstinduzierte Abflussinstationaritäten und Energiedissipation. Ph.D. Thesis, RWTH Aachen University, Aachen, Germany, 2008.
32. Cui, H.; Felder, S.; Kramer, M. Multilayer Velocity Model Predicting Flow Resistance of Aerated Flows Down Grass-Lined Spillway. *J. Hydraul. Eng.* **2022**, *148*, 06022014. [CrossRef]
33. Nepf, H.; Ghisalberti, M. Flow and transport in channels with submerged vegetation. *Acta Geophys.* **2008**, *56*, 753–777. [CrossRef]
34. Nepf, H.M. Hydrodynamics of vegetated channels. *J. Hydraul. Res.* **2012**, *50*, 262–279. [CrossRef]
35. Kothyari, U.C.; Hayashi, K.; Hashimoto, H. Drag coefficient of unsubmerged rigid vegetation stems in open channel flows. *J. Hydraul. Res.* **2009**, *47*, 691–699. [CrossRef]
36. Mossa, M.; Ben Meftah, M.; de Serio, F.; Nepf, H.M. How vegetation in flows modifies the turbulent mixing and spreading of jets. *Sci. Rep.* **2017**, *7*, 6587. [CrossRef]
37. Murphy, E.; Ghisalberti, M.; Nepf, H. Model and laboratory study of dispersion in flows with submerged vegetation. *Water Resour. Res.* **2007**, *43*, 1–12. [CrossRef]
38. Bai, R.; Ning, R.; Liu, S.; Wang, H. Hydraulic Jump on a Partially Vegetated Bed. *Water Resour. Res.* **2022**, *58*, e2022WR032013. [CrossRef]
39. Henderson, F.M. *Open Channel Flow*; Macmillan: New York, NY, USA, 1966.
40. Sena Fael, C.M.; Augusto Vaz Santos, C.; Batista Taborda, C.S. Flow velocity structure and turbulence characteristics in a partially vegetated channel with rigid emergent vegetation. In *Solo e Recursos Hídricos: Conservação, Recuperação e Manejo*; Da Melo Júnior, A.S., Ed.; Editora Artemis: Curitiba, Brazil, 2022; p. 65.
41. Steuernagel, J. Möglichkeiten zur Optimierung von Sanierungsmaßnahmen an Flussdeichen. Ph.D. Thesis, Technische Universität Darmstadt, Darmstadt, Germany, 2008.
42. Li, Y.; Wang, Y.; Anim, D.O.; Tang, C.; Du, W.; Ni, L.; Yu, Z.; Acharya, K. Flow characteristics in different densities of submerged flexible vegetation from an open-channel flume study of artificial plants. *Geomorphology* **2014**, *204*, 314–324. [CrossRef]

43. Velasco, D.; Bateman, A.; Redondo, J.M.; DeMedina, V. An Open Channel Flow Experimental and Theoretical Study of Resistance and Turbulent Characterization over Flexible Vegetated Linings. *Flow Turbul. Combust.* **2003**, *70*, 69–88. [CrossRef]
44. Järvelä, J. Flow resistance of flexible and stiff vegetation: A flume study with natural plants. *J. Hydrol.* **2002**, *269*, 44–54. [CrossRef]
45. Adeli, A.; Ahadiyan, J.; Ghomeshi, M.; Moghadam, M.R. Experimental study of two phase Air-water Flow Parameters in Hydraulic Jumps with vegetated Rough Bed. *Iran. J. Ecohydrol.* **2021**, *8*, 763–775.
46. *DIN 19712*; Hochwasserschutzanlagen an Fließgewässern (Flood Protection Works on Rivers). Beuth-Verlag: Berlin, Germany, 2013.
47. Chanson, H. Air-Water Flow Measurements with Intrusive, Phase-Detection Probes: Can We Improve Their Interpretation? *J. Hydraul. Eng.* **2002**, *128*, 252–255. [CrossRef]
48. Biethman, B.; Ettema, R.; Thornton, C.; Hogan, T.; Lan, Y. Air Entrained in Flow along a Steep-Stepped Spillway: Data and Insights from a Hydraulic Model. *J. Hydraul. Eng.* **2021**, *147*, 05021001. [CrossRef]
49. Felder, S.; Chanson, H. Phase-detection probe measurements in high-velocity free-surface flows including a discussion of key sampling parameters. *Exp. Therm. Fluid Sci.* **2015**, *61*, 66–78. [CrossRef]
50. Kramer, M.; Hohermuth, B.; Valero, D.; Felder, S. Best practices for velocity estimations in highly aerated flows with dual-tip phase-detection probes. *Int. J. Multiph. Flow* **2020**, *126*, 103228. [CrossRef]
51. Felder, S.; Pfister, M. Comparative analyses of phase-detective intrusive probes in high-velocity air–water flows. *Int. J. Multiph. Flow* **2017**, *90*, 88–101. [CrossRef]
52. Pagliara, S.; Felder, S.; Boes, R.M.; Hohermuth, B. Intrusive effects of dual-tip conductivity probes on bubble measurements in a wide velocity range. *Int. J. Multiph. Flow* **2024**, *170*, 104660. [CrossRef]
53. Hohermuth, B.; Kramer, M.; Felder, S.; Valero, D. Velocity bias in intrusive gas-liquid flow measurements. *Nat. Commun.* **2021**, *12*, 4123. [CrossRef]
54. Kramer, M.; Valero, D.; Chanson, H.; Bung, D.B. Towards reliable turbulence estimations with phase-detection probes: An adaptive window cross-correlation technique. *Exp. Fluids* **2019**, *60*, 2. [CrossRef]
55. EurOtop. Manual on Wave Overtopping of Sea Defences and Related Structures: An Overtopping Manual Largely Based on European Research, but for Worldwide Application. 2018. Available online: https://www.overtopping-manual.com/eurotop/downloads/ (accessed on 23 October 2024).
56. Wood, I.R.; Ackers, P.; Loveless, J. General Method for Critical Point on Spillways. *J. Hydraul. Eng.* **1983**, *109*, 308–312. [CrossRef]
57. Boes, R.M.; Droz, P.; Leroy, R. *Role of Dams and Reservoirs in a Successful Energy Transition, Proceedings of the 12th ICOLD European Club Symposium 2023 (ECS 2023), Interlaken, Switzerland, 5–8 September 2023*; Taylor & Francis Group: Milton, UK, 2023.
58. Felder, S.; Severi, A.; Kramer, M. Self-Aeration and Flow Resistance in High-Velocity Flows Down Spillways with Microrough Inverts. *J. Hydraul. Eng.* **2023**, *149*, 04023011. [CrossRef]
59. Arosquipa Nina, Y.; Shi, R.; Wüthrich, D.; Chanson, H. Air–Water Flows and Head Losses on Stepped Spillways with Inclined Steps. *J. Irrig. Drain Eng.* **2022**, *148*, 04022037. [CrossRef]
60. Bai, R.; Zhang, F.; Liu, S.; Wang, W. Experiments on Turbulence Intensity and Bubble Frequency in Self-Aerated Open Channel Flows. *Water* **2018**, *10*, 1201. [CrossRef]
61. Chanson, H.; Felder, S. Energy Dissipation on Embankment Dam Stepped Spillways, Overflow Stepped Weirs and Masonry Stepped Spillways. In Proceedings of the 17th Congress of IAHR Asia and Pacific Division, Auckland, New Zealand, 21–24 February 2010.